


## Article

# Study on the Atomization Characteristics of Flat Fan Nozzles for Pesticide Application at Low Pressures

Shougen Li , Chongchong Chen, Yaxiong Wang, Feng Kang and Wenbin Li \*

Key Lab of State Forestry Administration for Forestry Equipment and Automation, School of Technology, Beijing Forestry University, Beijing 100083, China; li\_shougen@bjfu.edu.cn (S.L.); chenrongchong@bjfu.edu.cn (C.C.); yaxiongwang87@bjfu.edu.cn (Y.W.); kangfeng98@bjfu.edu.cn (F.K.)

\* Correspondence: leewb@bjfu.edu.cn; Tel.: +86-10-62336137-709

**Abstract:** Spraying is the most widely used means of pesticide application for pest control in agriculture and forestry. The atomization characteristics of the nozzles are directly related to the spray drift, rebound, and deposition. Previous research studies have mainly focused on the change pattern of atomization characteristics. Mathematical descriptions of the atomization characteristics of flat fan nozzles are rare, and pesticide application theories are also insufficient. Atomization characteristics mainly include droplet size and velocity. This study analyzes the influence of the spray parameters (spray angle, pressure, and equivalent orifice diameter of nozzles) and the spatial position in the flow field. To obtain the atomization characteristics of flat fan nozzles, the phase Doppler particle analyzer (PDPA) was selected for the accurate measurement of the droplet sizes and velocities at distances 0.30–0.60 m, using low spray pressures (0.15–0.35 MPa). The droplet size and velocity models were then established and validated. The results revealed that the average absolute error of the droplet size model was 23.74  $\mu\text{m}$  and the average relative error was 8.23%. The average absolute and relative errors of the droplet velocity model were 0.37 m/s and 7.86%, respectively. At a constant spray pressure and angle, there was a positive correlation between the droplet size and the equivalent orifice diameter of the nozzles. The test also verified that the spray angle and distance had a negative correlation with the droplet velocity at a given pressure. The spray distance had no effect on the spray axial droplet size at constant spray pressure. In addition, the spray angle greatly affected the droplet velocity along the X-axis; similarly, the spray parameters, especially spray angle, greatly affected the droplet size.

**Keywords:** droplet velocity; droplet size; spray axis; long axis; PDPA; spray cross-section



check for updates

**Citation:** Li, S.; Chen, C.; Wang, Y.; Kang, F.; Li, W. Study on the Atomization Characteristics of Flat Fan Nozzles for Pesticide Application at Low Pressures. *Agriculture* **2021**, *11*, 309. <https://doi.org/10.3390/agriculture11040309>

Academic Editor: Massimo Cecchini

Received: 24 January 2021

Accepted: 31 March 2021

Published: 2 April 2021

**Publisher's Note:** MDPI stays neutral with regard to jurisdictional claims in published maps and institutional affiliations.



**Copyright:** © 2021 by the authors. Licensee MDPI, Basel, Switzerland. This article is an open access article distributed under the terms and conditions of the Creative Commons Attribution (CC BY) license (<https://creativecommons.org/licenses/by/4.0/>).

## 1. Introduction

In pesticide application using sprayers, the atomization characteristics of the nozzles play an important role in pesticide utilization [1–3]. While small-sized droplets have good deposition and coverage, they easily drift [4]. Droplet velocities also influence pesticide utilization; for example, droplets with very low velocities fail to reach the targets and those with very high velocities are prone to rebounding [5–7]. Therefore, understanding and mastering the atomization characteristics are important for using pesticide sprayers in agriculture and forestry.

Since the 1930s, researchers have studied the atomization characteristics of different nozzle outlet shapes (circular, square, rectangular, triangular, and elliptical) from two-dimensional spray to three-dimensional spray. Based on a study of the breaking mechanism of liquid films, Dombrowski and coworkers established the relationship between spray pressure and droplet size; they observed that the higher the pressure, the smaller the droplet, [8,9]. Sforza found that the droplet velocity along the spray direction decreased as a power function law and that the atomization characteristics between spray cross-sections along the spray direction were similar [10]. By measuring the droplet velocity and size at

0.50 m from the nozzle exit, Nuyttens found that the nozzle type and size had a significant effect on droplet velocity and size. Droplet velocities consistently decreased with the decrease in droplet size when the droplets were below a size of 400  $\mu\text{m}$  [11,12]. Yao studied the droplet size distribution of nozzles with different equivalent orifice diameters using a PDPA and observed that the Sauter mean diameter (SMD) was nonlinearly, but positively, correlated with the nozzle orifice diameter [13]. Xia performed water-air impinging jet tests and the impinging angle was  $90^\circ$  [14]. The atomization characteristics in the far and near fields were then analyzed. The results showed that SMD was smallest in the spray center and increased toward the spray edge. Xia also showed that the droplet velocity was the highest at the spray center and decreased gradually with increasing distance from the spray center. Kooij confirmed the parameters that determined the droplet size during the breaking of liquid films [15]. The results showed that fluid inertia and surface tension determined the droplet size, and the droplet size could be predicted using the Weber and nozzle parameters. Based on assumption that the flow field is two-dimensional, Kang established a droplet size model using an actual test and theoretical calculation and a droplet velocity model along the spray axis using numerical simulation and theoretical calculation [16]. Kang also indicated that the droplet size did not change significantly at distances of 0.30–0.50 m. Although several studies have been done on atomization characteristics, simple mathematical models are still very rare in far-field field at low pressures.

Because of their large spray range, flat fan nozzles are widely used in pesticide application in agriculture and forestry, especially in field spray and forest barrier treatment [17]. The flow field of flat fan nozzles is fan-shape and the spray cross-section is the elliptic [18]. The long axis determines the spray range during pesticide spraying, and based on the droplet characteristics along the long axis, the droplet characteristics along the short axis can be analyzed. Thus, the droplet characteristics along the spray axis and the long axis in the flow field are of profound significance in the study on the atomization characteristics of the whole field.

This study was conducted to establish the exact droplet size and velocity models on the long axis plane of flat fan nozzles based on the spray pressure, angle, and equivalent orifice diameter. According to the atomization model on the long axis plane, it is easy for workers to obtain the desired atomization effect by adjusting the spray pressure and the nozzle type, thereby improving the utilization rate of pesticides. Additionally, this research compensates for the shortcomings of the atomization theory in pesticide application, provides a method for further establishing a perfected atomization model of flat fan nozzles, and serves as a resource for subsequent research on droplet rebounding and deposition while hitting a given target. This study also provides a theoretical method for establishing atomization models of other nozzles, including conical, square, and rectangular nozzles.

## 2. Materials and Methods

### 2.1. Selection of Flat Fan Nozzle Types

Currently, the mainstream brands of flat fan nozzles available on the market include Teejet (Wheaton, IL, USA), Lechler (Metzingen, Germany), and Feizhuo (Shanghai, China), which are widely used in surface treatment, food industry, environmental protection, and pesticide spraying in agriculture and forestry. The internal structure of the 75 nozzles (Table 1) corresponding to the three brands were mapped using the Coordinate Measuring Machine (Leader NC8107, Wuxi Meider Measurement Technology Co., Jiangsu, China). The internal structure of the outlet of the nozzles of the three brands was cylindrical and ellipsoidal (Figure 1). Compared with the other two brands, the Teejet nozzle is more widely used in agriculture and forestry, and the commonly used angles are relatively large. Therefore, the 25 types of Teejet flat fan nozzles in Table 1 were selected for pesticide application in this study.

**Table 1.** Nozzle types of the three brands for mapping. The flow rate increases in the order of AT to ET, AF to EF, and AL to EL. At a pressure of 0.30 MPa, AT–ET are 0.79, 1.18, 1.58, 1.97, and 2.37 L/min, AF–EF are 0.79, 1.20, 1.60, 1.90, and 2.40 L/min, and AL–EL are 0.77, 1.23, 1.53, 1.96, and 2.33 L/min.

Manufacturer	Flow Rate Class	$d$	$\alpha$				
			25	40	65	80	110
Teejet	AT	0.80	2502	4002	6502	8002	11002
	BT	1.00	2503	4003	6506	8003	11003
	CT	1.20	2504	4004	6504	8004	11004
	DT	1.40	2505	4005	6505	8005	11005
	ET	1.50	2506	4006	6506	8006	11006
Manufacturer	Flow Rate Class	$d$	$\alpha$				
			25	40	65	80	110
Feizhuo	AF	0.91	2502	4002	6502	8002	11002
	BF	1.10	2503	4003	6506	8003	11003
	CF	1.30	2504	4004	6504	8004	11004
	DF	1.40	2505	4005	6505	8005	11005
	EF	1.60	2506	4006	6506	8006	11006
Manufacturer	Flow Rate Class	$d$	$\alpha$				
			30	45	60	90	120
Lechler	AL	1.00	632.362	632.363	632.364	632.366	632.367
	BL	1.20	632.402	632.403	632.404	632.406	632.407
	CL	1.35	632.442	632.443	632.444	632.446	632.447
	DL	1.50	632.482	632.483	632.484	632.486	632.487
	EL	1.65	632.512	632.513	632.514	632.516	632.517

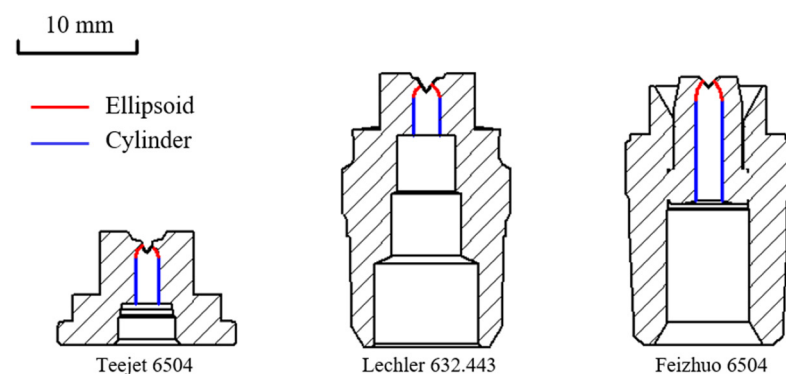


**Figure 1.** Sections showing the internal structure of the Teejet, Lechler, and Feizhuo nozzles.

## 2.2. Basic Theory

The findings of this study would mainly serve pesticide application using sprayers in agriculture and forestry. Since the droplet size distribution function is very complicated, the average droplet size has been used as one of the spray characteristics [19]. In this study, we used the volume mean diameter ( $D_v$ ) as the average droplet size, which is the most commonly used average diameter in the analysis of the spray characteristics in pesticide spraying [20].  $D_v$  is calculated as follows:

$$D_v = \left( \frac{\int_{D_{\min}}^{D_{\max}} D^3 dN}{\int_{D_{\min}}^{D_{\max}} dN} \right)^{\frac{1}{3}} \quad (1)$$

The droplet velocity is expressed in terms of the average velocity as follows:

$$u = \frac{\int_{U_{\min}}^{U_{\max}} U dN}{\int_{U_{\min}}^{U_{\max}} dN} \quad (2)$$

Based on the nozzle size and spray pressure, a function model of droplet size was obtained by Post [21] as follows:

$$D_v \propto \left(\frac{FR}{01}\right)^{\frac{1}{3}} P^{-\frac{1}{3}} \left(\frac{\alpha}{110^\circ}\right)^{-\frac{2}{3}} \quad (3)$$

Under a stable field, since the probabilities of breakage and fusion of droplets are greatly reduced, the influence of spray distance on atomization characteristics can be neglected. In addition, the change rule of droplet size along the Z-axis was similar to that in the flow field:

$$D_z = C_v d^p P^{-\frac{1}{3}} \alpha^q \quad (4)$$

Sforza proposed that the droplet velocity along the Z-axis decreases as an exponential function and was related to the ratio of the spray distance and minor axis of the elliptical opening [10]. The observation can be mathematically expressed as

$$\frac{u_z}{u_0} \propto z^{-m} \quad (5)$$

$$\frac{u_z}{u_0} \propto f\left(\frac{z}{b}\right) \quad (6)$$

The effective hydraulic area ( $A_{hyd}$ ) and  $b$  satisfied the following function:

$$b = \sqrt{\frac{2A_{hyd}}{3\pi}} \quad (7)$$

where  $A_{hyd} = C_D A$  in which  $A = \pi d^2 / 4$ .

The pressure and velocity of the nozzle outlet and inlet satisfy the Bernoulli equation, and the velocity changes caused by gravity and the nozzle inlet velocity are negligible [22]. The droplet velocity along the spray distance is given as follows:

$$u_z \propto P^{\frac{1}{2}} z^m d^n \quad (8)$$

The relationship between the maximum droplet size and velocity satisfies a power function under a stable field. From Equation (4), the function of droplet velocity along the Z-axis based on the spray angle could be obtained as follows:

$$u_z = C_u P^{\frac{1}{2}} z^m d^n \alpha^l \quad (9)$$

To better understand the atomization characteristics along the X-axis, the dimensionless quantities  $D_x/D_z$  and  $u_x/u_z$  were introduced. Previous research studies have indicated that the droplet size along the X-axis satisfies a quadratic function and the droplet velocity a Gaussian distribution:

$$\frac{D_x}{D_z} = A_x x^2 + B_x x + C_x \quad (10)$$

$$\frac{u_x}{u_z} = a_x e^{-\frac{(x-x)^2}{2w_x^2}} \quad (11)$$

### 2.3. Experimental Design

#### 2.3.1. Test System Composition

All experiments were conducted at the Mining Science Center, China University of Mining and Technology, Xuzhou, China. The data acquisition system is shown in Figure 2. The system mainly comprised the PDPA system (TSI, Inc., Shoreview, MI, USA) and a 1WZB-25Z PRODN pressure pump (Intelligent Electronic Technology Co., Zhejiang, China) for providing stable pressure. A 3DOF mobile platform was used to control the PDPA position precisely. Additionally, the system included flow meters, pressure gauges, and nozzle holders.

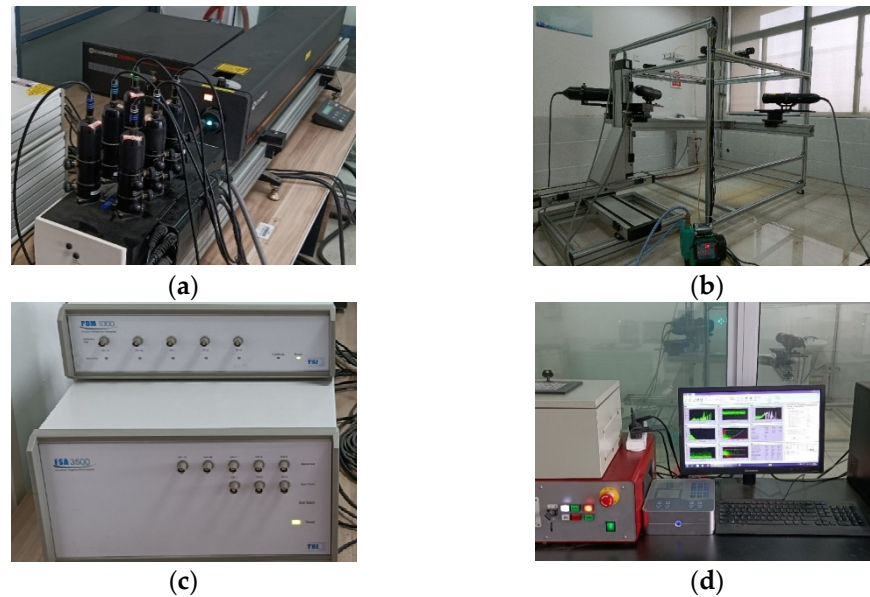


**Figure 2.** Test system: (a) laser and multicolor beam separator; (b) the transmitting probe and receiver along with 3DOF mobile platform; (c) signal processor; and (d) computer with the FLOWSIZETM software installed.

#### 2.3.2. Test Methods

This study is an investigation of the basic model. Tests were conducted indoors with no wind at a stable temperature and humidity so that the amount of droplet evaporation could be ignored. To minimize the influence of gravity, the nozzles were arranged in a downward direction (Figure 3). To clearly describe the characteristics, a rectangular coordinate system in space was established with the nozzle exit center as the coordinate origin. The X, Y, and Z axes represent the long and short axes of the spray cross-section and the spray axis, respectively. Seven horizontal spray cross-sections were selected along the Z-axis ranging from 0.30 to 0.60 m with an interval of 0.05 m. Different intervals along the X-axis were chosen for data acquisition on horizontal planes based on the spray angles of the flat fan nozzles. An interval of 0.01 m was chosen for flat fan nozzles with spray angles 25° and 40° and 0.02 m for the ones with spray angles 65°, 80°, and 110°. The preset pressure values were 0.15, 0.20, 0.25, 0.30, and 0.35 MPa. Three replicates were conducted at each measurement point, and at least 5000 droplets were measured per replicate to ensure the data accuracy of the measurement. The average of the three replicates was used as the droplet size and velocity at the measurement position.



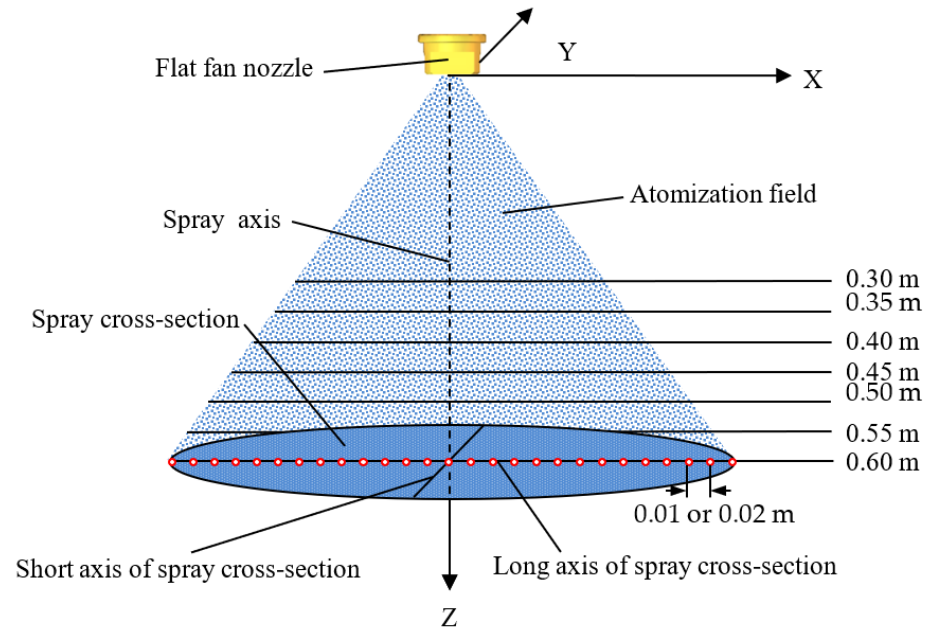


**Figure 3.** Field of flat fan nozzles. The small red circles represent the measurement point.

### 3. Results and Discussion

For uniform coverage, adjacent fields are made to overlap by 50–100% when pesticides are being sprayed. To understand the flow field of flat fan nozzles, three nozzles were selected for measurement at different spray pressures and distances. The atomization characteristics for different cross-sections of the five nozzles with the same flow rate at pressure 0.25 MPa and 0.50 m away from the nozzle outlet are shown in Figure 4, which validates previous research [23–25]. The results indicated that the change trend of the droplet size and velocity was the same for the three nozzles. The droplet size was observed to be smaller at the center and larger at the edge. The droplet velocity was found to be the highest at the center of the flow field and decreased gradually toward the edge. These cases also showed that the changes in the droplet size and velocity on the spray cross-section were continuous and symmetrical in the spray center. The characteristics of the droplets along the long axis could be linked to those at the center of the cross-section. In the following, the part of the flow field with  $x > 0$  will be analyzed.

In this section, the establishment of the droplet size and velocity models on the XZ plane are mainly discussed and the same method was used to establish the droplet size and velocity on the XZ plane. Firstly, by fitting part of the experimental data with the single variable method, the coefficients in Equations (4), (9)–(11) were determined. Then, the exact droplet characteristic models on the XZ plane were obtained. Finally, the models were validated by other experimental data.

#### 3.1. Establishment of the Droplet Size Model

##### 3.1.1. Droplet Size Model on Z-Axis

In the flow field, the droplet size is related to the spray pressure, spray angle, equivalent orifice diameter, and spatial position. The distributions between the droplet size along the Z-axis and different spray parameters are shown in Figures 5–8.

As can be seen in Figure 5, there were no noticeable changes in the droplet size and spray distance among the nine nozzles that were selected. This occurred because the droplets were not easily blended and they ran along the original motion trajectory after the liquid film broke twice and formed stable droplets. Additionally, the evaporation of the droplets could basically be ignored through the measurement range. Therefore, the droplet size hardly changed along the Z-axis, and the droplet size was independent of the spray distance. For this reason, in the process of establishing the droplet size model along the

Z-axis, we took the average droplet size at the seven spray distances under certain spray parameters as the droplet size.

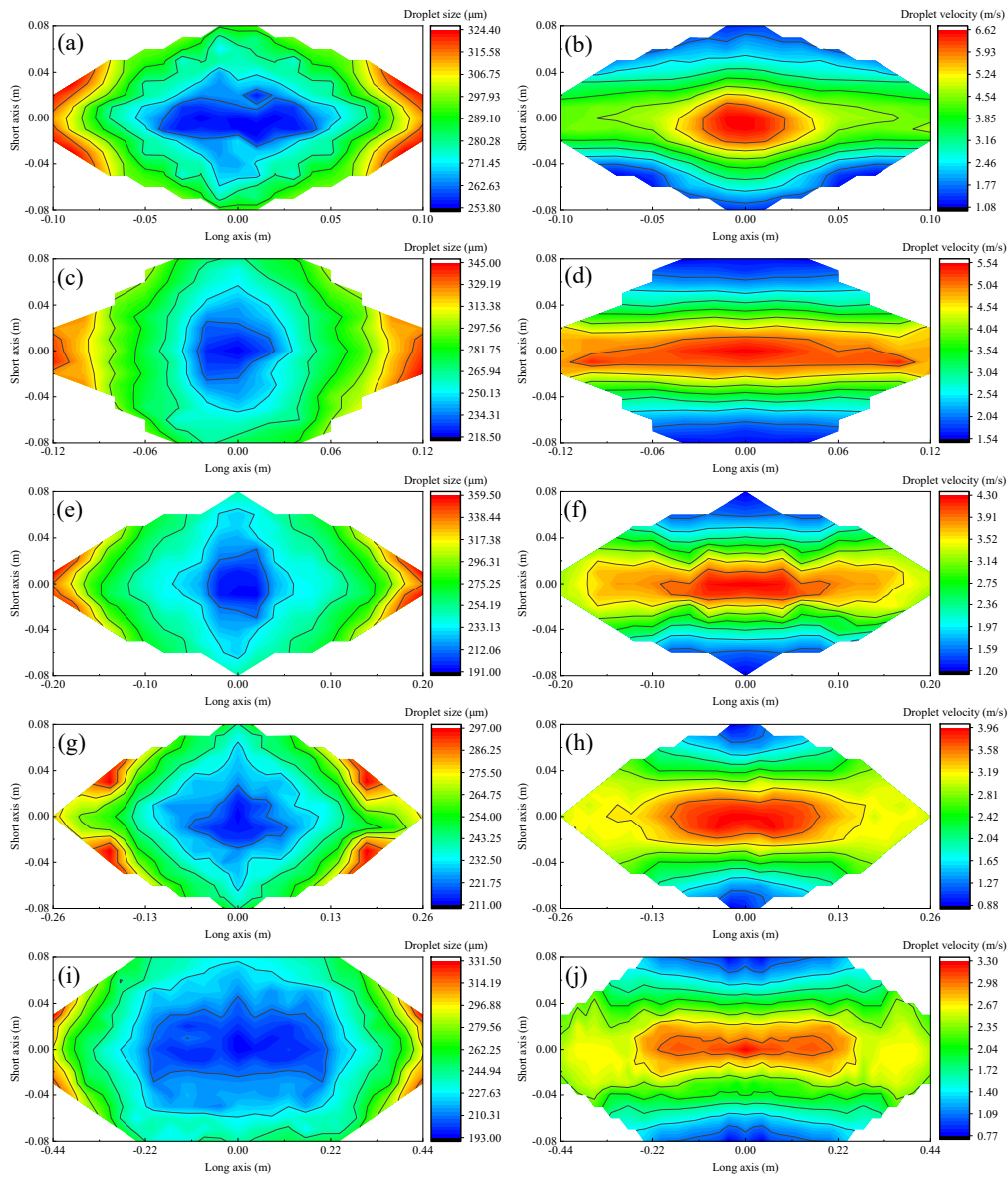


Figure 4. Cloud chart of droplet size and velocity for five flat fan nozzles at 0.25 MPa and 0.50 m away from the nozzle outlet: (a,b) 2504; (c,d) 4004; (e,f) 6504; (g,h) 8004; and (i,j) 11004.

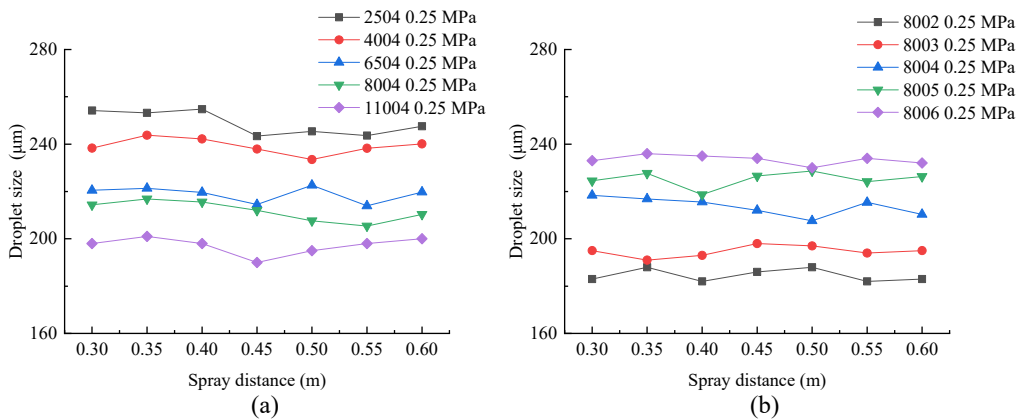


Figure 5. Graph of droplet size vs. spray distance: (a) different spray angles; and (b) different flow rates.

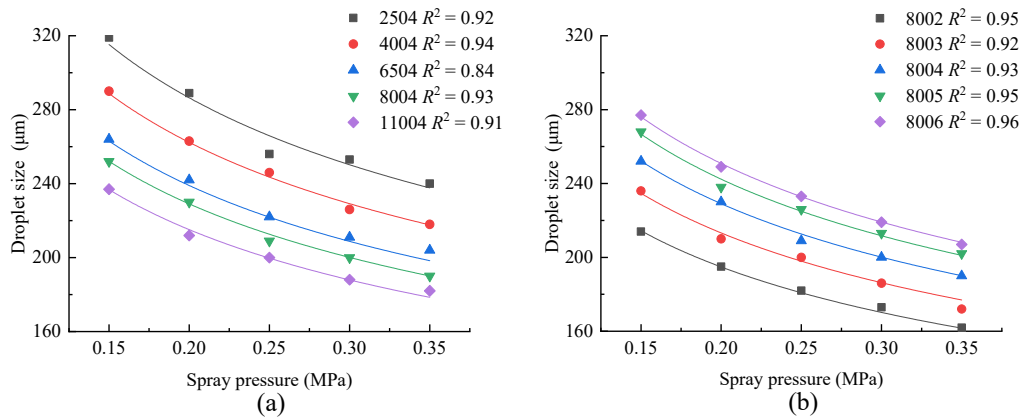


Figure 6. Fitting curves and values of droplet size vs. spray pressure: (a) different spray angles; and (b) different flow rates.

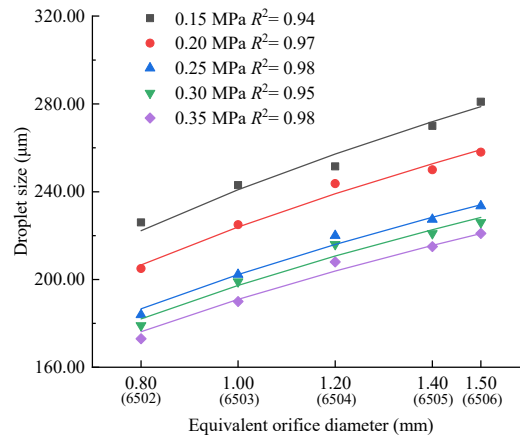


Figure 7. Fitting curves and values of droplet size vs. equivalent orifice diameter.

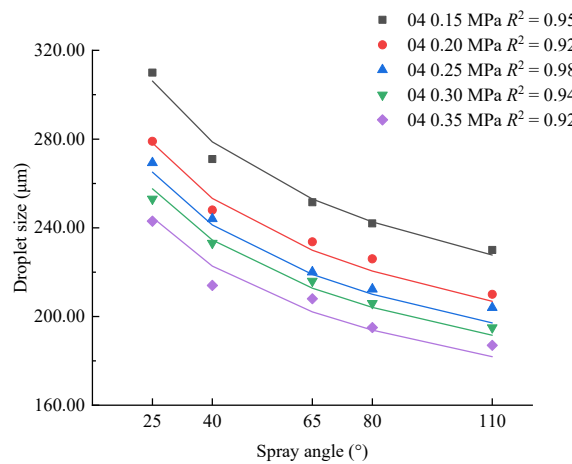


Figure 8. Fitting curves and values of droplet size vs. spray angle.

As can be seen in Figure 6, the droplet size along the Z-axis gradually decreased with the increase in the spray pressure. According to the Bernoulli equation, the droplet velocity at the nozzle outlet increases with the increase in the spray pressure, causing the liquid film to break to produce smaller droplets. The fitting function between the droplet size along the Z-axis and the spray pressure is represented as follows:

$$D_z \propto P^{-\frac{1}{3}} \tag{12}$$



As can be seen in Figure 7, the droplet size along the Z-axis was positively correlated with the equivalent orifice diameter for nozzles 6502, 6503, 6504, 6505, and 6506 at five different pressure values. The fitting function between the droplet size along the Z-axis and the equivalent orifice diameter is represented as follows:

$$D_z \propto d^{\frac{2}{5}} \tag{13}$$

The relationship between the spray angle and the droplet size at different pressure values with the same equivalent orifice diameter is shown in Figure 8. The droplet size along the Z-axis decreased with the increase in the spray angle. At constant spray pressure and flow rate, the increase in the spray angle was observed to lead to a decrease in the thickness of the liquid film after liquid ejection, with the thickness of the film was positively correlated with the size of the droplet formed after breaking. Therefore, the larger the spray angle, the smaller the droplet size. The fitting function between the spray angle and the droplet size along the Z-axis is represented as follows:

$$D_z \propto \alpha^{-\frac{1}{5}} \tag{14}$$

The droplet size model along the Z-axis (Equation (15)) was obtained from Equations (12)–(14). The value of coefficient  $C_v$  was 300, which was obtained by measuring the droplet size of nozzle 6504 at 0.15 MPa.

$$D_z = C_v \alpha^{-\frac{1}{5}} P^{-\frac{1}{3}} d^{\frac{2}{5}} \tag{15}$$

### 3.1.2. Droplet Size Model on the X-Axis

The dimensionless quantity  $D_x/D_z$  along the X-axis is shown in Figure 9. Since the droplet size along the X-axis is centrosymmetric,  $B_x = 0$  and  $C_x = 1$ . This section further explores the relationship between  $A_x$  and the spray parameters based on the experimental data.

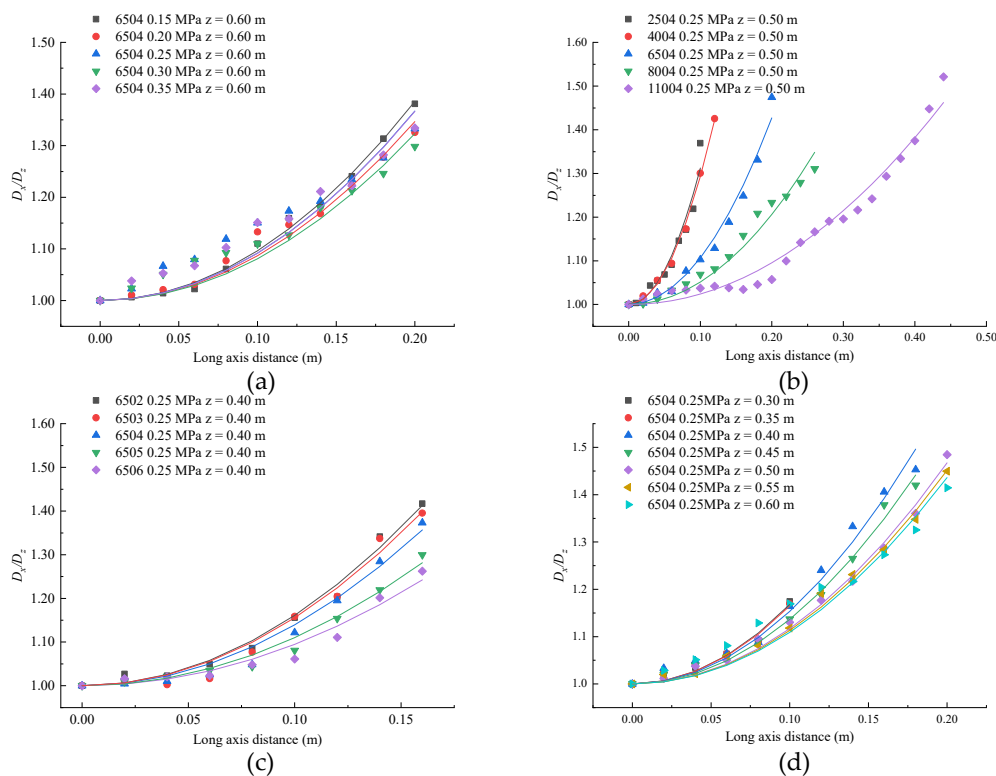


**Figure 9.** Fitting curves of  $D_x/D_z$  along the X-axis with different parameters: (a) spray pressure; (b) spray angle; (c) equivalent orifice diameter; (d) spray distance.

As can be seen from Figure 9, the spray pressures, spray angles, equivalent orifice diameters, and spray distances were correlated with  $D_x/D_z$ , and the size of the droplets at the center was smaller than the size of the droplets at the edge along the X-axis under different spray parameters. It can be seen from Figure 9a that the spray pressure had no effect on the change trend of the droplet size along the X-axis. Figure 9b–d indicates that the dimensionless quantity decreased greatly with the decrease in the spray angle, equivalent orifice diameter, and spray distance. Without considering the influence of evaporation and drift, the larger the difference in the droplet velocities at the center and the edge of the flow field, the more small droplets were entrained in the center, which led to the faster change of droplet size along the X-axis. Therefore, the change in the droplet size along the X-axis was more uniform with the increase in the spray angle, equivalent orifice diameter, and spray distance.

The data were fitted using Equation (10), and the  $A_x$  values are shown in Table 2 for different spray parameters. From Table 2, it can be observed that the  $A_x$  values for spray angle  $65^\circ$  fluctuated between 8.08 and 16.79, with an average of 12.20. Further, the values varied greatly based on the spray angle. Therefore, the  $A_x$  values determined using spray angles are listed in Table 3 to facilitate validation.

**Table 2.**  $A_x$  and the fitting degrees for different spray parameters.

6504 z = 0.60 m		
$P$	$A_x$	$R^2$
0.15	9.64	0.99
0.20	8.67	0.98
0.25	9.18	0.85
0.30	8.08	0.91
0.35	9.16	0.89
P = 0.25 MPa z = 0.50 m		
$\alpha$	$A_x$	$R^2$
2504	31.22	0.95
4004	29.34	0.99
6504	11.68	0.98
8004	5.15	0.96
11004	2.39	0.97
P = 0.25 MPa z = 0.40 m		
$d$	$A_x$	$R^2$
6502	16.13	0.98
6503	15.55	0.96
6504	13.94	0.98
6505	11.51	0.97
6506	9.47	0.93
6504 P = 0.25 MPa		
$z$	$A_x$	$R^2$
0.30	16.79	0.98
0.35	16.46	0.95
0.40	15.32	0.98
0.45	13.63	0.99
0.50	11.69	0.99
0.55	11.29	0.96
0.60	10.91	0.92

**Table 3.**  $A_x$  values based on the spray angle.

$\alpha$	25	40	65	80	110
$A_x$	31.00	29.00	12.00	5.00	2.00

3.2. Establishment of the Velocity Model

3.2.1. Droplet Velocity Model on the Z-Axis

This section analyzes the droplet velocity along the Z-axis with respect to spray pressure, spray distance, spray angle, and equivalent orifice diameter using Equation (9).

Figure 10 shows the droplet velocities along the Z-axis at different spray distances from the selected five nozzles. For all five flat fan nozzles, the droplet velocity was observed to gradually decrease with the increase in the spray distance; this was because after the breakage of the liquid film and formation of the stable droplets, the kinetic energy of each droplet decreased due to the air resistance, and thus the droplet’s velocity also decreased. In addition, the velocity reduction rate was also observed to decrease gradually with the increase in the spray distance. The reason for the phenomenon was that the air resistance of the droplet was inversely proportional to the square of its velocity. The lower the droplet velocity, the smaller the air resistance. The mathematical function of the best fit curve between the droplet velocity along the Z-axis and the spray distance was obtained using the following equation:

$$u_z \propto z^{-\frac{3}{5}} \tag{16}$$

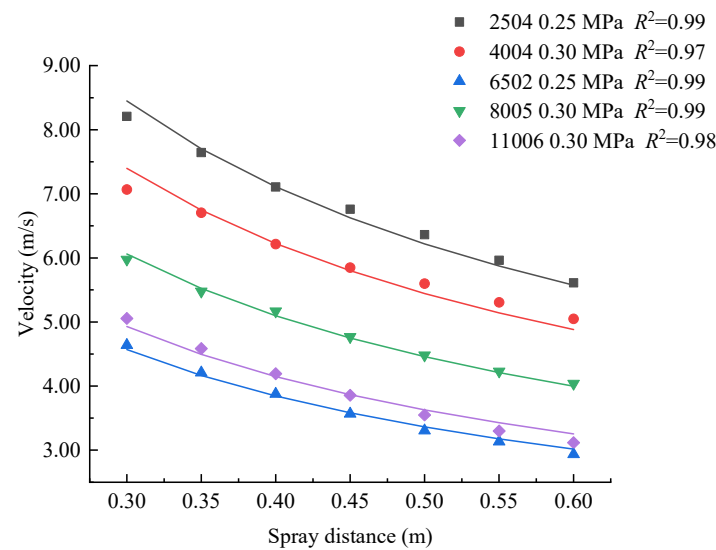


**Figure 10.** Fitting curves of droplet velocity vs. spray distance.

As can be seen from Figure 11, the droplet velocity along the Z-axis decreased with the increase in the spray angle at a pressure of 0.25 MPa, and the reduction rate was decreased. The spray coverage increased with the increase in the spray angle, subjecting the droplets to greater air resistance, so the droplet velocity in the flow field of nozzles with a large spray angle was less than that in the flow field of nozzles with a small spray angle given the same spray distance. The central entrainment decreased with the increase in the spray angle, which caused fewer droplets with small velocity to move from the edge into the central region. Therefore, the reduction in droplet velocity decreased with the increase in the spray angle. The fitting function between the spray angle and droplet velocity is represented as follows:

$$u_z \propto \alpha^{-\frac{1}{2}} \tag{17}$$

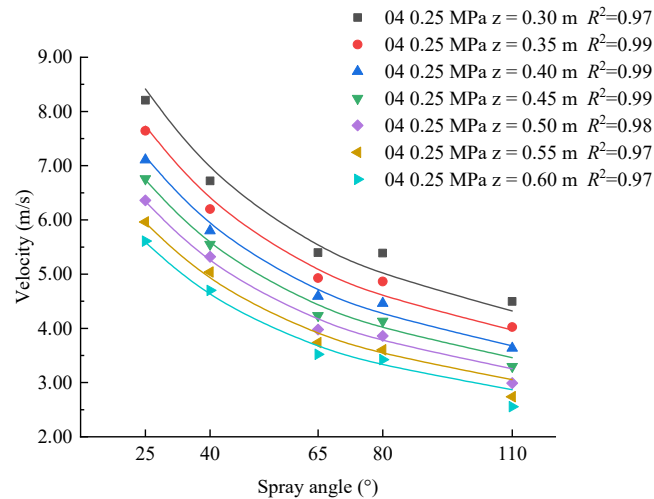


Figure 11. Fitting curves of droplet velocity vs. spray angle.

As can be seen in Figure 12, the droplet velocity along the Z-axis increased with the increase in the equivalent orifice diameter at a constant spray angle of 65°. The fitting function between the equivalent orifice diameter and droplet velocity is represented as follows:

$$u_z \propto d^{\frac{2}{5}} \tag{18}$$

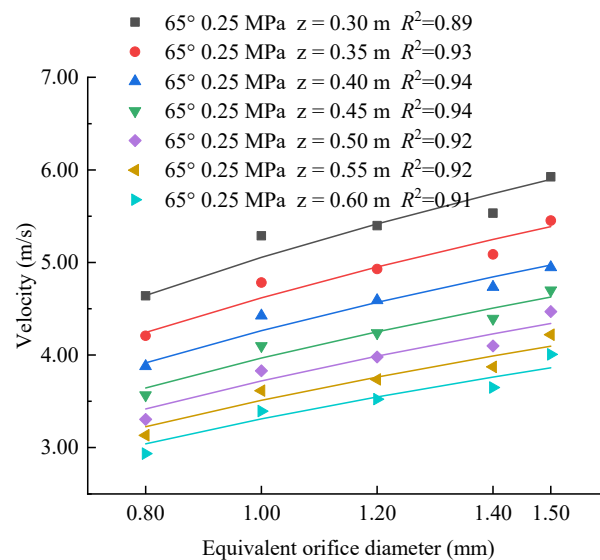


Figure 12. Fitting curves of droplet velocity vs. equivalent orifice diameter.

The droplet velocity model along the Z-axis (Equation (19)) was obtained from Equations (16)–(18). The value of coefficient  $C_u$  was 40, which was obtained by measuring the droplet velocity of nozzle 6504 at 0.15 MPa.

$$u_z = C_u P^{\frac{1}{2}} z^{-\frac{3}{5}} d^{\frac{2}{5}} \alpha^{-\frac{1}{2}} \tag{19}$$

### 3.2.2. Droplet Velocity Model on the X-Axis

The dimensionless quantity  $u_x/u_z$  along the X-axis is shown in Figure 13. Since the droplet velocity along the X-axis is centrosymmetric,  $x_x = 0$  and  $a_x = 1$ . This section further explores the relationship between  $w_x$  and the spray parameters based on the experimental data.

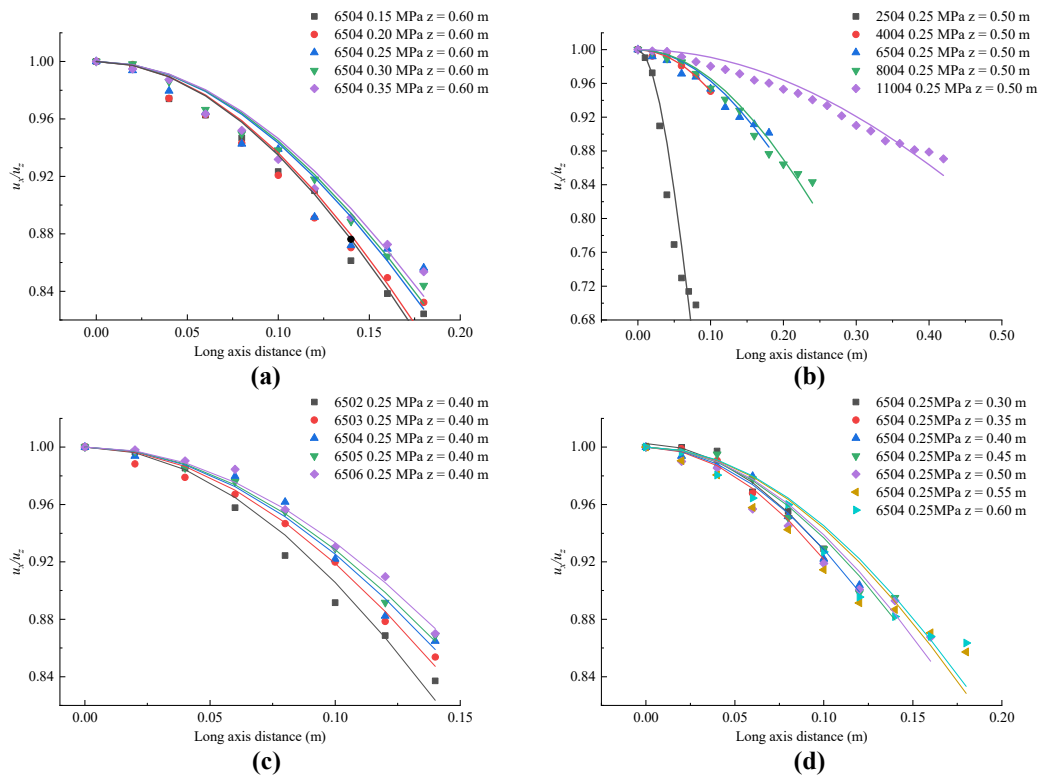


**Figure 13.** Fitting curves of  $u_x/u_z$  along the X-axis at different spray parameters: (a) spray pressure; (b) spray angle; (c) equivalent orifice diameter; and (d) spray distance.

As can be seen from Figure 13, the spray pressures, spray angles, equivalent orifice diameters, and spray distances were correlated with  $u_x/u_z$ , and the velocity of the droplets at the center was higher than that of the droplets at the edge along the X-axis. The dimensionless curve with respect to the different spray parameters showed that the decrease in the droplet velocities along the X-axis was more severe with the decrease in the spray pressure, spray angle, and equivalent orifice diameters. This is because the difference in the velocities of the droplets at the center and the edge may lead to an entrainment of the low-velocity droplets from the edge to the central area; since a higher number of low-velocity droplets are entrained at the center when the difference is large, the reduction rate of the velocity of the droplets along the X-axis increases with the decrease in the spray pressure, angle, and equivalent orifice diameter. Because of environmental resistance, the droplet velocities at the cross-section are expected to be gradually consistent with the increase in the spray distance, which explains why the velocities along the X-axis decreased slowly with the increase in the spray distance.

The  $w_x$  values and fitting degrees for different spray parameters are shown in Table 4, after fitting the data using Equation (11). From Table 4, it can be seen that the  $w_x$  values for nozzles with  $65^\circ$  fluctuated between 0.22 and 0.30, with an average of 0.27. However, the  $w_x$  values varied greatly based on the spray angle. The  $w_x$  values determined using the spray angle are shown in Table 5.

### 3.3. Validation of the Models

In this section, two groups of nozzles were used to validate the droplet size and velocity models. One group with the same flow rate (CT) and different spray angles (25, 40, 65, 80, and 110) was verified at 0.20 MPa and 0.50 m away from the nozzle outlet, and the other group with the same spray angle (80) and different flow rates (AT, BT, CT, DT, and ET) was verified at 0.25 MPa and 0.50 m away from the nozzle outlet. A comparison of the error values between the measured and theoretical data on the size and velocity of the droplets along the X-axis is shown in Figures 14 and 15, respectively. The figures

show that the error occurred mainly at a point away from the spray center and that the error corresponding to nozzle 2502 was very large. The main reason for the increase in the error is the small number of droplets and their unstable nature at the edges. The large error of nozzle 2502 is due to the influence of the nozzle structure on the increase rate of surface wave length in the transition part of the jet spray. The nozzle outlet with a small spray angle has a small aspect ratio, which improves the increase rate of the surface wave wavelength, causes a larger interval width in the transition part, and intensifies the instability of nozzle atomization [26]. Additionally, machining accuracy may also be a reason for the large error. The errors corresponding to the measured and theoretical data were further analyzed, as shown in Table 6. The average absolute error for droplet size was 23.74  $\mu\text{m}$ , and the average relative error was 8.23%. The average absolute and average relative errors corresponding to the droplet velocity were 0.37 m/s and 7.86%, respectively.

**Table 4.**  $w_x$  and the fitting degrees for different spray parameters.

6504 $z = 0.60$ m		
$P$	$w_x$	$R^2$
0.15	0.28	0.92
0.20	0.28	0.94
0.25	0.29	0.90
0.30	0.30	0.98
0.35	0.30	0.95
$P = 0.25$ MPa $z = 0.50$ m		
$\alpha$	$w_x$	$R^2$
2504	0.08	0.88
4004	0.32	0.97
6504	0.28	0.91
8004	0.38	0.96
11004	0.74	0.92
$P = 0.25$ MPa $z = 0.40$ m		
$d$	$w_x$	$R^2$
6502	0.22	0.98
6503	0.24	0.99
6504	0.25	0.98
6505	0.26	0.99
6506	0.27	0.99
6504 $P = 0.25$ MPa		
$z$	$w_x$	$R^2$
0.30	0.26	0.97
0.35	0.25	0.99
0.40	0.26	0.98
0.45	0.28	0.96
0.50	0.28	0.91
0.55	0.29	0.86
0.60	0.30	0.90

**Table 5.**  $w_x$  values based on the spray angle.

$\alpha$	25	40	65	80	110
$w_x$	0.08	0.32	0.28	0.38	0.74



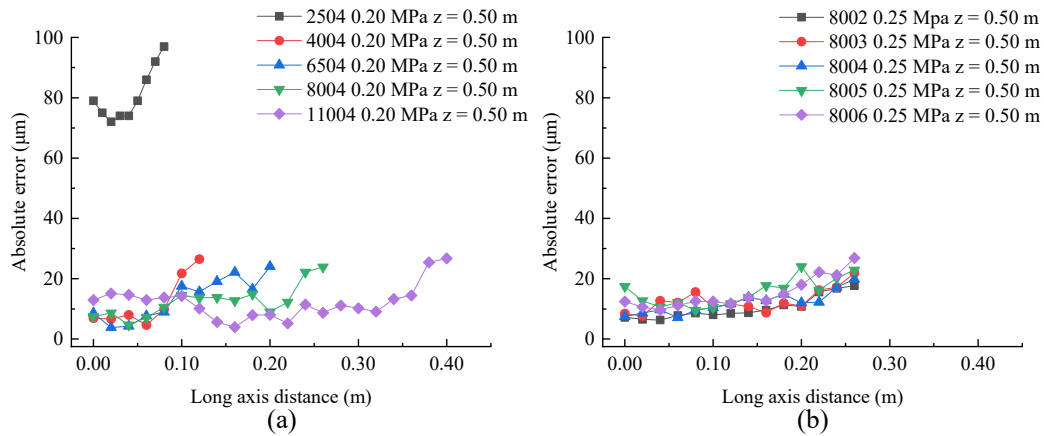


**Figure 14.** Absolute errors between the measured and theoretical data corresponding to the droplet size: (a) different spray angles; and (b) different flow rates.

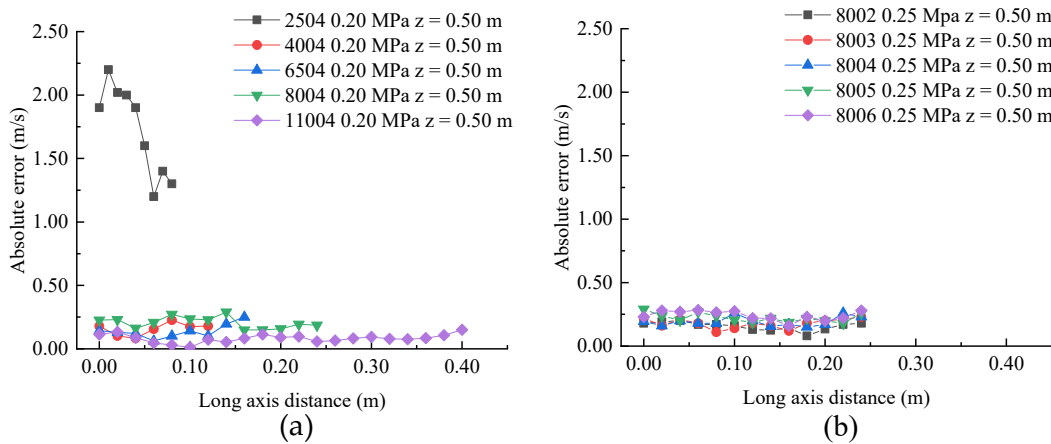


**Figure 15.** Absolute errors between the measured and theoretical data corresponding to the droplet velocity: (a) different spray angles; and (b) different flow rates.

**Table 6.** Errors of measured and theoretical data.

	Absolute Error	Relative Error
$D_x$	23.74 $\mu\text{m}$	8.23%
$u_x$	0.37 m/s	7.86%

**4. Conclusions**

Based on the theoretical derivation and actual tests, this study established the exact droplet size and velocity models on the XZ plane. According to this model, it is easier for workers to obtain the desired spray size and speed by adjusting the spray pressure and nozzle type during pesticide spraying, so as to improve the spray effect. The results of the validation revealed that the average absolute error and average relative error corresponding to the droplet size model were 23.74  $\mu\text{m}$  and 8.23%, respectively, and the average absolute error and average relative error corresponding to the droplet velocity model were 0.37 m/s and 7.86%, respectively. Thus, the theoretical atomization model was suitable for the actual test results. In addition, this study also illustrated that the droplet size was higher at the center than at the edge in the flow field, and the maximum difference exceeded 50%. The droplet velocity model showed the opposite change trend, and the maximum difference exceeded 30%. The spray angle greatly influenced the atomization characteristics along the X-axis. From the atomization characteristics, it was found that the increase in the spray angle could increase the droplet uniformity under the condition of ensuring spray volume.

This study provides a method to further explore atomization models on the short axis and to establish complete three-dimensional atomization models.

**Author Contributions:** Conceptualization, S.L. and W.L.; methodology, S.L.; software, S.L.; validation, S.L., C.C. and Y.W.; formal analysis, S.L.; investigation, F.K.; resources, F.K.; data curation, S.L. and C.C.; writing—original draft preparation, S.L.; writing—review and editing, Y.W.; visualization, S.L.; supervision, Y.W.; project administration, F.K.; funding acquisition, W.L. All authors have read and agreed to the published version of the manuscript.

**Funding:** This work was supported by the National Key R&D Program of China, grant number 2018YFD0700603.

**Acknowledgments:** We thank LetPub ([www.letpub.com](http://www.letpub.com), 10 December 2020) for linguistic assistance during the preparation of this manuscript.

**Conflicts of Interest:** No conflict of interest exists in the submission of this manuscript, and the manuscript has been approved by all authors for publication. I would like to declare on behalf of my co-authors that the work described is original research that has not been published previously and is not under consideration for publication elsewhere, in whole or in part. All the authors listed have approved this manuscript.

## Nomenclature

$a_x$	the coefficients related to spray parameters
$A_{hyd}$	effective hydraulic area (mm <sup>2</sup> )
$B$	the minor axis of the elliptical orifice (mm)
$C_D$	a coefficient
$C_v$	the constant related to the spray parameters
$d$	equivalent orifice diameter (mm)
$D_{max}$	maximum droplet size (μm)
$D_v$	volume mean diameter (mm)
$D_z$	the droplet size along the Z-axis (μm)
$l$	a coefficient
$n$	a coefficient
$p$	a coefficient
$q$	a coefficient
$u_0$	the velocity at the nozzle orifice (m/s)
$u_z$	the droplet velocity along the Z-axis (m/s)
$U_{min}$	minimum droplet velocity (m/s)
$w_x$	the coefficients related to spray parameters
$x_x$	the coefficients related to spray parameters
$\alpha$	spray angle (°)
$A$	the true orifice area (mm <sup>2</sup> )
$A_x$	a coefficient
$B_x$	the coefficients related to spray parameters
$C_u$	a constant related to the spray parameters
$C_x$	the coefficients related to spray parameters
$D$	the droplet size (μm)
$D_{min}$	minimum droplet size (μm)
$D_x$	the droplet size along the X-axis (μm)
$FR$	flow rate class of the nozzle
$m$	the coefficient
$N$	the number of droplets
$P$	the spray pressure (MPa)
$u$	average droplet velocity (m/s)
$u_x$	the droplet velocity along the Z-axis (m/s)
$U_{max}$	maximum droplet velocity (m/s)
$U$	the droplet velocity (m/s)
$x$	coordinate value along the X-axis (m)
$z$	coordinate value along the Z-axis (m)

## References

1. Heick, T.M.; Hansen, A.L.; Munk, L.; Labouriau, R.; Wu, K.; Jørgensen, L.N. The effect of fungicide sprays on powdery mildew and rust and yield of sugar beet in Denmark. *Crop. Prot.* **2020**, *135*, 105199. [[CrossRef](#)]
2. Paudel, S.; Sah, L.; Devkota, M.; Poudyal, V.; Prasad, P.; Reyes, M. Conservation Agriculture and Integrated Pest Management Practices Improve Yield and Income while Reducing Labor, Pests, Diseases and Chemical Pesticide Use in Smallholder Vegetable Farms in Nepal. *Sustainability* **2020**, *12*, 6418. [[CrossRef](#)]
3. Warneke, B.W.; Zhu, H.; Pscheidt, J.W.; Nackley, L.L. Canopy spray application technology in specialty crops: A slowly evolving landscape. *Pest. Manag. Sci.* **2020**. [[CrossRef](#)]
4. Zhang, B.; Tang, Q.; Chen, L.-P.; Zhang, R.-R.; Xu, M. Numerical simulation of spray drift and deposition from a crop spraying aircraft using a CFD approach. *Biosyst. Eng.* **2018**, *166*, 184–199. [[CrossRef](#)]
5. Subr, A.K.; Sawa, J.; Parafiniuk, S. Practical Deviation in Sustainable Pesticide Application Process. *Agric. Agric. Sci. Procedia* **2015**, *7*, 241–248. [[CrossRef](#)]
6. Ferguson, J.C.; Chechetto, R.G.; Adkins, S.W.; Hewitt, A.J.; Chauhan, B.S.; Kruger, G.R.; O'Donnell, C.C. Effect of spray droplet size on herbicide efficacy on four winter annual grasses. *Crop. Prot.* **2018**, *112*, 118–124. [[CrossRef](#)]
7. Preftakes, C.J.; Schleier, J.J.; Kruger, G.R.; Weaver, D.K.; Peterson, R.K. Effect of insecticide formulation and adjuvant combination on agricultural spray drift. *PeerJ* **2019**, *7*, e7136. [[CrossRef](#)] [[PubMed](#)]
8. Dombrowski, N.; Fraser, R.P. A Photographic Investigation into the Disintegration of Liquid Sheets. In *Philosophical Transactions of the Royal Society A: Mathematical, Physical and Engineering Sciences*; Royal Society of London, England: London, UK, 1954; Volume 247, pp. 101–130.
9. Dombrowski, N.; Johns, W. The aerodynamic instability and disintegration of viscous liquid sheets. *Chem. Eng. Sci.* **1963**, *18*, 203–214. [[CrossRef](#)]
10. Sforza, P.M.; Steiger, M.H.; Trentacoste, N. Studies on three-dimensional viscous jets. *AIAA J.* **1966**, *4*, 800–806. [[CrossRef](#)]
11. Nuyttens, D.; Baetens, K.; De Schampheleire, M.; Sonck, B. Effect of nozzle type, size and pressure on spray droplet characteristics. *Biosyst. Eng.* **2007**, *97*, 333–345. [[CrossRef](#)]
12. Nuyttens, D.; De Schampheleire, M.; Verboven, P.; Brusselman, E.; DeKeyser, D. Droplet Size and Velocity Characteristics of Agricultural Sprays. *Trans. ASABE* **2009**, *52*, 1471–1480. [[CrossRef](#)]
13. Yao, C.; Geng, P.; Yin, Z.; Hu, J.; Chen, D.; Ju, Y. Impacts of nozzle geometry on spray combustion of high pressure common rail injectors in a constant volume combustion chamber. *Fuel* **2016**, *179*, 235–245. [[CrossRef](#)]
14. Xia, Y.; Khezzar, L.; Alshehhi, M.; Hardalupas, Y. Droplet size and velocity characteristics of water-air impinging jet atomizer. *Int. J. Multiph. Flow* **2017**, *94*, 31–43. [[CrossRef](#)]
15. Kooij, S.; Sijts, R.; Denn, M.M.; Villermaux, E.; Bonn, D. What Determines the Drop Size in Sprays? *Phys. Rev. X* **2018**, *8*, 031019. [[CrossRef](#)]
16. Kang, F.; Wang, Y.; Li, S.; Jia, Y.; Li, W.; Zhang, R.; Zheng, Y. Establishment of a static nozzle atomization model for forest barrier treatment. *Crop. Prot.* **2018**, *112*, 201–208. [[CrossRef](#)]
17. Virginia Cooperative Extension, Virginia Tech. Nozzles: Selection and Sizing. Available online: <https://vtechworks.lib.vt.edu/bitstream/handle/10919/93422/BSE-262.pdf?sequence=1> (accessed on 22 April 2019).
18. Vallet, A.; Tinet, C. Characteristics of droplets from single and twin jet air induction nozzles: A preliminary investigation. *Crop. Prot.* **2013**, *48*, 63–68. [[CrossRef](#)]
19. Mugele, R.; Evans, H.D. Droplet size distributions in sprays. *Ind. Eng. Chem.* **1951**, *43*, 1317–1324. [[CrossRef](#)]
20. Cao, J. *Liquid Sprays*; Peking University Press: Beijing, China, 2013; pp. 200–225.
21. Post, S.L.; Hewitt, A.J. Flat-Fan Spray Atomization Model. *Trans. ASABE* **2018**, *61*, 1249–1256. [[CrossRef](#)]
22. Zhou, Q.; Miller, P.; Walklate, P.; Thomas, N. Prediction of Spray Angle from Flat Fan Nozzles. *J. Agric. Eng. Res.* **1996**, *64*, 139–148. [[CrossRef](#)]
23. Zhang, J.; Song, J.; He, X.; Zeng, A. Droplets movement characteristics in atomization process of flat fan nozzle. *Trans. Chin. Soc. Agric. Mach.* **2009**, *42*, 66–69, 75.
24. Kashani, A.; Parizi, H.; Mertins, K. Multi-step spray modelling of a flat fan atomizer. *Comput. Electron. Agric.* **2018**, *144*, 58–70. [[CrossRef](#)]
25. Nadeem, M.; Chang, Y.K.; Venkatadri, U.; Diallo, C. Water quantification from sprayer nozzle by using particle image velocimetry (piv) versus imaging processing techniques. *Pak. J. Agric. Sci.* **2018**, *55*, 203–210.
26. Gong, C.; Ou, M.; Jia, W. The effect of nozzle configuration on the evolution of jet surface structure. *Results Phys.* **2019**, *15*. [[CrossRef](#)]